X-625-76-219

PREPRINT

EMPIRICAL MODELS OF HIGH LATITUDE ELECTRIC FIELDS

J. P. HEPPNER

SEPTEMBER 1976

GSFC

GODDARD SPACE FLIGHT CENTER
GREENBELT, MARYLAND

Empirical Models of High Latitude Electric Fields

J. P. Heppner

September 1976

Abstract

Model cross-sections of the high latitude dawn-dusk electric field based on OGO-6 data are presented for the "signature" profiles (Heppner, 1972c) most frequently encountered for both + and -Y orientations of the interplanetary magnetic field. Line integrals give a total potential of 76 kev in each case. The median magnetic disturbance for these models is Kp ≐ 3. To illustrate extremes, examples of model cross-sections with total potentials of 23 kev and 140 kev are also given for periods of Kp = 0 and AE ≐ 1000, respectively. Model convection patterns are also presented utilizing OGO-6 data on boundary locations at other magnetic local times. When this information is combined with characteristic field geometries in the region of the Harang discontinuity, and is supplemented by data from Ba^+ cloud motions in the polar cap, it becomes possible to construct realistic convection patterns on the nightside which deviate from the usual sun-aligned patterns. These modifications are essential because, in general, it is not possible to maintain sun-alignment and obtain convective continuity with the geometries observed in the midnight region.

The need for empirical models is evident when observations are compared with typical theoretical models. In particular, observed field distributions at and near the polar cap boundary do not resemble the distributions frequently used in theory. The observational models presented are also of limited applicability as a consequence of the variability of observed distributions. These limitations are emphasized with particular attention given to several types of recurrent deviations which have not previously been discussed.

INTRODUCTION

It is generally recognized that existing theoretical models of the global electric field are not realistic because of their inability to describe space-time variations (e.g., see conference review by Olson, 1975). It is not as commonly recognized that most models have gross average characteristics which are not in agreement with observations. Although there are exceptions (e.g., Maeda, 1976) the use of electric field data in model making has seldom extended beyond selection of a latitude for placing a boundary between anti-solar and solar directed convective flows, and the choice of a magnitude for the potential drop across the polar cap, anti-solar flow region (e.g., Wolf, 1974; Volland, 1975; Kawasaki, 1975). The over-simplification has been a necessary first step but it can be misleading particularly when the consequences of differences between model and observed fields are not evaluated in interpreting results from analyses based on simple models. Because simple models have been extensively used, examples are too numerous to cite here. One can, however, note examples of major differences which will consistently affect a user's results in that they are persistent differences and not just a function of the variability. Two such differences are illustrated by Figure 1 which shows: (a) the most simple form of the dawn-dusk $\underline{E}$ field from observations discussed later in this paper, and (b) a typical form of theoretical model fields, adapted from Volland (1975) by adjusting the magnitude scale. It is obvious that the boundary between polar cap, anti-solar convection and auroral belt, solar directed convection is quite different for the two dawn-dusk sections. It is similarly obvious in looking at measurements, and Figure 1, that maximum field intensities in

the belt of solar directed convection occur within the belt and not at its polar cap boundary as depicted in most theoretical models. Other types of examples appear relative to models which depict fast convection adjacent to the plasmapause at all local times.

Construction of the observational models presented here was partially motivated by an apparent need for illustration of differences such as those noted above. More positive motivations came from: (a) the authors own need for representative convection pictures to illustrate the distribution of ion drag forces producing related patterns of high latitude ionospheric winds, (b) the belief that these models will be useful to others, and (c) interest in looking at the geometry required to obtain continuity in connecting flow across the dawn-dusk meridian to the complex flow patterns observed in the vicinity of the Harang discontinuity. The emphasis here is on the distribution and geometry of the convection flow. It is not, however, possible to derive an electric field model with general validity. Based only on characteristic distributions of the dawn-dusk polar cap field it was previously found (Heppner, 1972c) that with 12 "signature" classifications of the distribution it was still necessary to use combinations of signatures to categorize one-third of the OGO-6 polar cap traverses. Occurrences of the different signatures are not, however, equally likely and within the OGO-6 data from June 1969 several characteristic distributions are dominant. With the objective being the construction of the simplest possible convection patterns, quantitatively based on the OGO-6 measurements, the two most frequently observed northern hemisphere (summer) distributions are presented in model form. These two (Signatures A and B in Heppner, 1972c) occur, respectively, when the interplanetary

magnetic field (IMF) is in the - or +Y hemisphere in solar-ecliptic coordinates so dependence on the azimuthal direction of the interplanetary magnetic field is taken into account. The data selection is also such that both models are representative of conditions which produce magnetic disturbance levels of Kp ≤ 3. To dispel any pretense that these models have general applicability and to illustrate a greater range of conditions, model cross-sections are also shown for two select time periods when the fields were exceptionally weak and strong and were, respectively, accompanied by magnetic conditions Kp = 0 and AE ≤ 1000.

OGO-6 provides accurate measurements of the horizontal component of the electric field normal to the sun-line along orbits which provide essentially a dawn-dusk cross-section. With this information one can construct sun-aligned convection patterns resembling the original idealizations of Axford and Hines (1961) to obtain convective continuity within the observed boundaries. The result, however, is not realistic in representing observations near the Harang discontinuity in the nightside auroral belt. Thus, one must modify the pattern based on dawn-dusk data to fit typical conditions near the Harang discontinuity as determined by the OGO-6 data taken during satellite eclipse (Maynard, 1974), barium ion cloud motions, and various analyses of aurora and magnetic observatory data (Heppner, 1972a). This introduces a geometry for convective flow in the nightside auroral belt which does not permit a direct connection with anti-solar polar cap flow unless one invokes a deviation from the anti-solar direction in the nightside polar cap. Fortunately, a suitable form for this deviation is in agreement with tracks of Ba^+ clouds released from rockets in the nightside polar cap.

In the midday sector between 70 and 80° invariant latitude, it is possible that characteristic flow geometries exist which are analogous to those in the midnight auroral belt. There is not, however, adequate data to supplement the dawn-dusk OGO-6 data to justify alterations in the large scale sun-aligned features of the flow pattern. Fields in this region are typically highly irregular with numerous large amplitude, small scale fluctuations and field reversals superimposed on the general pattern (Heppner, 1972b; 1973). Thus, the neglect of small scale features in modeling is likely to be of greater consequence in the midday sector than elsewhere.

OGO-6 DATA AND PREVIOUS MODELS

To avoid repetition the reader is referred to Heppner (1972b) for descriptions and discussions of the instrumentation, the quantities measured, accuracies and limitations, the distribution of data in magnetic coordinates as determined by the orbit and season, some of the differences between northern (summer) and southern (winter) hemisphere fields, and a preliminary look at boundary locations taken prior to the signature classification of dawn-dusk cross-sections which is presented in Heppner (1972c). A detailed account of boundary locations and peak magnitudes as related to IMF parameters and additional information on summer-winter differences appears in Heppner (1973). Measurements at auroral latitudes near midnight have been presented by Maynard (1974) where 10 OGO-6 passes through this region are shown. Examples of measured fields along dawn-dusk, polar traverses of OGO-6 are available in a number of papers and thus are omitted here (e.g., see, 16 polar passes in Heppner, 1972b; 4 in Heppner, 1972c; 7 in Heppner, 1973; 6 in Heppner, 1972d; 19 in Langel,

1975; and mosaics of 21 passes in Gurnett, 1972, and Cauffman and Gurnett, 1972).

Global modeling of the OGO-6 data exists in two imcompatible forms: the boundary location modeling by Heppner (1973), which neglects distributions in intensity, and the distribution models of Bohse and Aggson (1973) based on contour fitting to grids of average values without reference to boundary locations. Although complementary, these two approaches are imcompatible and understanding why they are imcompatible gives some insight into the reasons for the restrictive approach to modeling taken in this paper. The undesirable effect of using average grid values from many orbits is that the distribution is broadened in scale and reduced in amplitude relative to the actual distribution along most of the individual orbits. Specifically: (a) the low latitude boundary of the sunward convection zone is shifted equatorward to the lowest latitude encountered in an individual case, (b) the boundary transition from anti-solar to solar directed convection becomes a region of weak gradients as a result of algebraic canceling of oppositely directed dawn-dusk $\underline{E}$ fields from shifts in the boundary from orbit to orbit, and (c) peak magnitudes for the averaged field are less than those observed in most individual cases, again as a consequence of shifts in distribution between orbits.

CRITERIA AND ASSUMPTIONS IN DAWN-DUSK MODELING

Along each dawn-dusk polar traverse, peak magnitudes, locations of peak magnitudes, and boundary locations can be scaled independent of field intensity distributions. A basic premise in the present modeling is not only that these quantitative parameters be accurately represented

but also that they are to be regarded as being mutually dependent parameters. For example, locations of the polar cap boundary from a particular traverse are not used unless the peak magnitude and low latitude boundaries are also used for the same traverse. This restricts the data to traverses in which there are not data gaps and thus greatly reduces the information available on any one parameter. It is, however, essential for accurately representing the mutual relationships between the various boundaries and locations of maximum field intensities.

The least quantitative, and most questionable, aspect of the dawn-dusk modeling from OGO-6 is the selection of a model form for the gradients of the electric field between boundaries and the points of maximum field intensity within the morning and evening auroral belts. The fact that there is not a prevailing form is obvious from even a casual examination of the data. From orbit to orbit, for example, the distribution in crossing the auroral belt can range from having a broad smooth maximum to cases where there are pronounced irregularities such that the peak intensity is appreciably greater than average intensities near the peak value. In view of this diversity and from inspection of many orbits in addition to those used for model construction, it was decided that the most simple compromise representation would be one in which the gradients in $\underline{E}$ are constants over each region separating a peak from a boundary (i.e., a straight line increase or decrease in $\underline{E}$ with distance). After making this decision numerous passes were re-examined to see if, and where, this compromise might be misleading. This produced the opinion that the straight line compromise is reasonable in all the regions but is most questionable in the morning auroral zone between the field maximum

and the low latitude boundary. In this zone there is a dominance of cases where |E| decreases away from the maximum toward lower latitudes at a rate greater than given by a straight line representation.

The assumption is made that all non-zero equipotential contours are crossed twice in a satellite dawn-dusk traverse (i.e., that there are not flow paths which close entirely on just the day or just the night side of a given traverse). This introduces an unavoidable uncertainty but there are not alternatives that can be based on data. Errors from this assumption are kept to a minimum by restricting the data used for dawn-dusk profiles to passes which enter and leave the high latitude convection between 17 and 19 hours magnetic local time (MLT) and 5 and 7 hours MLT, respectively. The error, when present, will give a total potential difference that is less than the actual.

To obtain the most representative data set for a given signature, it is also necessary to eliminate satellite traverses where there is a localized feature that would cause the overall distribution for that traverse to be misrepresented. For example, if a peak intensity comes from a transient that is distinct from the region where the field has a broad maximum, or if a polar cap boundary crossing is highly irregular with a series of sign reversals, the data scaled would not accurately reflect the distribution. Thus, a subjective elimination of data has been applied to reduce the number of cross-sections to the most meaningful set for modeling.

Southern hemisphere data is not used for modeling the dawn-dusk distribution, in part because fewer orbits meet the MLT criteria, but also because field irregularities in many cases make signature classifications

more questionable as explained in Heppner (1972c). The southern hemisphere dayside boundary data are, however, used in later constructions of convection patterns.

DAWN-DUSK DISTRIBUTION: MODELS A AND B

Using the above criteria, the number of northern hemisphere traverses for modeling was reduced to 11 and 9, respectively, for Models A and B. In rough percentages this is only 12 percent of the northern hemisphere traverses but the 20 traverses become representative of 40 to 50 percent of the data when viewed in terms of the number of cross-sections meeting the MLT and completeness of data criteria. It is important to note that magnetic disturbance conditions were not used as a criteria. When examined after selection it was found that for the 11 signature A cases Kp ranged from 2^- to 5 with a median between Kp = 3 and 3^+. For the signature B cases Kp ranged from 2^+ to 4^+ with a median at Kp = 3. Thus the equivalence of magnetic disturbance levels is a fortunate coincidence.

The 4 boundary locations, 3 peak magnitudes, and 3 locations of the peak magnitudes were scaled for each of the polar crossings and then averaged. Mean values and standard deviations, σ, are listed in Table 1. An exception is the location of the peak magnitude in the polar cap for signature A as this is relatively random for the flat distribution and is thus meaningless when averaged. The average peak magnitude in the signature A polar cap is also not very meaningful as it is influenced by small irregularities. Its value and standard deviation are listed, with asterisks, primarily to illustrate the limited range of variability.

The steps taken in converting the mean values of Table 1 to Models A and B shown in Figures 2 and 3, respectively, are most readily apparent

in the case of B. The first step is to see how well the sum of the line integrals for the evening and morning auroral belts matches the line integral across the polar cap using the actual mean values and the straight line, constant gradient, approximation discussed previously. This step is simplified by assuming a constant satellite altitude of 500 km in place of the actual 400-600 km range over the latitudes of interest. The error introduced by the altitude assumption is less than 5 percent and is probably less than the error that might be expected from the straight line approximation. As shown in Table 1 the sum of the evening (subscript 18) and morning (subscript 6) line integrals, 76800 volts, is within 9 percent of the polar cap integral, 83810 volts. The fact that the agreement is this close adds credence to this approach to modeling. For model simplicity the next step is to make the summation of line integrals equal to zero and also round off the magnitudes of the potential changes to convenient values. This involves minor adjustments of peak magnitudes, primarily in the polar cap, as given in Table 1. The cross-section distribution for $\underline{E}$ and the potential are shown in Figure 3.

In the case of Model A the magnitude of the polar cap field has to be calculated to make the polar cap line integral equal to the sum of the evening and morning auroral belt integrals. As shown in Table 1 this is done after rounding off the sum 40780 + 36490 = 77270 to the more convenient value, 76000, by making adjustments of $\leq$ 1.0 volts/km in the auroral belt peak magnitudes. The resulting cross-section distributions for $\underline{E}$ and the potential are shown in Figure 2.

There is not an obvious explanation for the remarkable equality, < 500 volts difference, between the Model A and Model B sums, 77270 and

76800, for the morning and evening auroral belt line integrals. The fact that the data selection criteria have very little influence on this agreement is borne out by the magnitudes of the standard deviations given in Table 1. Thus the closeness of the agreement is regarded as being fortuitous. It is, however, probably significant that the values are similar when one notes the similarity in the median values of Kp accompanying the two models. Essentially it implies that for a given total potential the two distributions produce roughly equal magnetic disturbances.

DAWN-DUSK DISTRIBUTIONS: QUIET AND DISTURBED EXAMPLES

During one of the few Kp = 0 time periods encountered by OGO-6 in June 1969, there were two successive northern hemisphere traverses with very similar field distributions of the type classified as signature C (Heppner, 1972c). The total potential associated with these traverses is either the minimum or very close to the minimum seen by OGO-6 for crossings meeting the MLT criteria. To show this minimum field condition, in the same form as used for A and B, the two traverses have been averaged by the same technique. The result is shown in Figure 4 as Model C(0). The rounding-off between mean and model magnitudes is only by 0.1 volts/km in the two sunward convection regions. The polar cap line integral is matched by adjusting the polar cap magnitude from a mean peak value of 23.3 to a model value of 21.4 volts/km and assigning a magnitude of 2.0 volts/km to the almost negligible field in the evening polar cap which characterizes signature C (Heppner, 1972c).

Selection of magnetically disturbed conditions for modeling in terms of signatures presents greater difficulties. Mixing data taken under high Kp conditions from different days does not yield a uniform set in terms of

signatures. In part this reflects the lack of time resolution in a 3-hour index, but it is also expected from the previous finding (Heppner, 1973) that a quantitative Kp dependence on E could not be accurately defined because of numerous exceptions. Thus the approach was taken of looking for a series of successive passes with large magnitude fields with similar signature characteristics. Six successive passes on June 12, 1969 come close to meeting this criteria with characteristics ranging between signatures A and D both of which occur in association with a +Y IMF (Heppner, 1972a). Kp values of 3^+, 5, and 4^- for this 9 hour period do not appear to reflect the degree of disturbance as well as the AE(11) index. The AE index reached 1000 twice during the interval and in terms of AE this is the most disturbed interval encountered by OGO-6 even through Kp's of 5 and 6^- appeared two days later. Thus this interval bridging the AE = 1000 condition was picked for representation.

Several compromises in the criteria used for Models A and B are necessary in using these 6 traverses, but large errors appear unlikely. For example, although ranging from signatures A to D the locations of peak fields in the polar cap are relatively random with 3 occurring on both the morning and the evening sides of the pole. Also, the D type asymmetry is not pronounced. Other compromises were: (a) auroral belt peak magnitudes from one traverse were not used because one of the two for that traverse occurred where there was missing data, (b) data was missing at two 18^h polar cap boundary crossings, and (c) data was missing at three $\Lambda(18)$ boundaries. In the case of the 3 missing $\Lambda(18)$ boundaries, locations were taken from the preceding conjugate southern hemisphere crossing of the same boundary on grounds that the locations were within the same hour in MLT. Unlike the $\Lambda(18)$ boundary

where conjugacy is a reasonable assumption, data substitution for the two missing polar cap boundaries would be misleading.

The result for the disturbed condition is shown in Figure 5 as Model AD. The rounding-off between mean and model values is such that the auroral belt line integrals change from 73470 to 73000 and 67070 to 67000 volts. A matching polar cap line integral of 140,000 volts is obtained by using 38.6 volts/km in place of the mean peak value of 45.2 volts/km. The mean peak polar cap field, of course, has limited meaning as explained relative to Model A.

Several points are obvious in comparing Models A and AD, Figures 2 and 5: (a) there is relatively little change in the locations of polar cap boundaries in the dawn-dusk meridian, (b) magnitudes are significantly greater for the disturbance model, and (c) the low latitude boundary of the convection has a pronounced shift to lower latitudes in the disturbance model. These features are identical to correlations, and lack of correlation in the case of polar cap boundaries, found relative to the magnitude and southward declination of the IMF in Heppner (1973). As the IMF was moderately strong and southward throughout most of this time period, the corresponding result could have been anticipated. The previous analysis did not, however, treat the location of peak magnitudes in the sunward convection, or auroral belt, regions. The present result indicates a complete lack of shifting in the morning peak but a moderate shift in the evening peak.

SUN-ALIGNED MODEL CONVECTION PATTERNS

In Figures 6(a) and 7(a) equipotential lines crossing the dawn-dusk meridians in Models A and B, respectively, are distributed as symmetrically

as possible within the boundaries of the convection electric field using the assumption that the polar cap convection is exactly anti-solar. For the placement of low latitude (zero potential) and polar cap (dashed line) boundaries at MLT's not encountered in polar passes between 17-19 hours and 5-7 hours MLT it is necessary to blend "typical" locations to the statiscally defined locstions between 17 and 19 hours and 5 and 7 hours because the signature classification loses meaning when the orbit does not cross-section the central polar region approximately normal to the sunline. These "typical" locations come from various approaches to the data; for example: (a) at midnight where northern hemisphere passes occur at $\Lambda \geq 70^\circ$ in June 1969 the low latitude (zero potential) boundary is estimated for Kp $\triangleq$ 3 from Maynard's (1974) study, (b) at noon where northern hemisphere passes occur at $\Lambda \geq 80^\circ$ and southern hemisphere passes occur at $\Lambda \geq 70^\circ$ the zero potential boundary is placed at 70° on grounds explained later, (c) also near noon, the polar cap boundary is placed slightly below 80° because the northern hemisphere passes consistently encounter polar cap fields above 80°, and a tabulation of southern hemisphere passes for Kp = 2 to 4 yielded an average of 79.4°, and (d) at MLT's between the four areas, 17-19 hours, 5-7 hours, midnight, and noon, median lines drawn on scatter plots of boundary locations are considered to be a good approximation to averages. The variability of boundaries with MLT is discussed further below relative to quiet and disturbed conditions.

Sun-aligned patterns for the quiet Model C(0) and disturbed Model AD cross-sections are shown in Figures 8 and 9, respectively, with equipotential contours of 2000 and 8000 volts in place of the 4000 volt contours used for Models A and B. Polar cap boundaries are purposely not indicated in Figures

8 and 9 because the data do not justify placing the AD boundary different than for A or the C(0) boundary different than that for B. In view of often expressed opinions that the polar cap expands and contracts with increasing and decreasing disturbance levels this may be surprising and thus require further documentation and explanation. For this purpose it is convenient to view the polar cap boundary behavior in the 17-19 and 5-7 hour zones separate from the behavior near midnight and noon. Comparing the A with the AD cross-section (Figures 2 and 5) and the B with the C(0) cross-section (Figures 3 and 4) the differences in polar cap boundary latitudes range from 0° to 1.2° which is well within the σ values given in Table 1. These small differences are consistent with the more general finding that the summer hemisphere polar cap boundary position at these local times is statistically independent of the IMF southward declination and magnitude except for a weak correlation with previous values of the southward declination (for details, see Heppner, 1973). The equivalence of Model B and Model C(0) polar cap boundaries in the 17-19 and 5-7 hour zones must, however, be viewed with caution because the related +Y IMF signature denoted by RC (Heppner, 1972c) introduces complications in interpretation as noted later.

The fact that grounds have not been found for significantly changing the noon and midnight polar cap boundaries as a function of disturbance level may be a consequence of the greater variability of the boundary at these local times. Particularly in the midnight sector it is known that auroral activity frequently expands poleward as well as equatorward during substorm enhancements. This dynamical behavior could easily produce a scatter of polar cap boundary locations that obscures average differences that might be found with continuous observations over long periods of time.

From OGO-6 orbits normal to the sunline near 71° near midnight (N. hemisphere) and near 79° near noon (S. hemisphere) one can only say that it appears almost equally likely that polar cap fields will be encountered, at least during a portion of the pass, whether the disturbance level is high or low. The path lengths and magnitudes where the polar cap fields appear are, however, likely to be greater when the disturbance level is high. In essence, this implies eddy structures with larger dimensions and field magnitudes under disturbed conditions. These cannot be represented in the smoothed models shown here.

In contrast to the polar cap boundary, it is known (Heppner, 1973) that the low latitude boundary at MLT's 17-19 and 5-7 hours is highly correlated with the magnitude and southward declination of the IMF and with magnetic disturbance conditions. Near midnight it is also known (Maynard, 1974) that the magnetic disturbance increases as this boundary shifts equatorward. It is not, however, obvious that the low latitude boundary location at noon is greatly different for high and low values of Kp. In fact, two characteristics of the southern hemisphere dayside data suggest that the location is confined to a small latitudinal range, 68 to 71°, at 12 hours MLT. One is that plots of the dayside low latitude boundary encounters for all levels of disturbance and IMF orientations show a convergence toward 70° and 12 hours MLT from a broader latitudinal scatter at earlier and later MLT's (i.e., the scatter of points in latitude decreases progressively toward 12 hours from both 6 and 18 hours). The other characteristic is that near 12 hours the observed fields are consistently weak below 72° (e.g., 5 - 10 volts/km as opposed to ≥ 20 volts/km). If the boundary was at a latitude much lower than 70° one would expect to occasionally find stronger fields

in this region. In view of these characteristics the boundary in Models A, B, and C(0) is shown at 70° at 12 hours MLT. In Model AD some allowance for a decreasing latitude with increasing disturbance is made by placing the 12 hour point at 68° but it appears equally probable that 70° could apply in this case as well.

Figures 6(b) and 7(b) show the effect of adding corotational potentials, $-91.2 \sin^2 \theta$ kilovolts, to the convection fields of Figures 6(a) and 7(a) using the approximation that the rotational axis, $\theta = 0°$, and invariant latitude pole coincide. The alternative to this approximation, making the models applicable to a specific universal time, was also attempted using the mean UT for the orbits entering into the A and B model cross-sections, but the increase in accuracy that this would imply between 17-19 hours and 5-7 hours MLT would obviously not apply at other MLT's where the data come from different UT intervals. Multiple satellites would be required to reveal UT modulations.

MODIFIED MODEL CONVECTION PATTERNS

The sun-aligned patterns in Figures 6(a) and 7(a), and similarly 6(b), 7(b), 8, and 9, are not in agreement with other observations on the night-side in three independent respects. First, as deduced from various observations (reviewed by Heppner, 1972a) and shown by OGO-6 (Maynard, 1974) the flow pattern in the midnight auroral belt does not closely resemble the simple sun-aligned split shown between evening and morning auroral belt regions. Instead, the reversal from westward flow (poleward E) in the evening to eastward flow (equatorward E) in the morning is seen with increasing latitude as well as increasing local time near midnight. The instantaneous configuration of this reversal, called the Harang discontinuity, varies

greatly with time but one can approximately represent its basic shape and location: for example, as indicated with dashed lines in Figures 6(c) and 7(c).

The second disagreement is that average magnitudes of the component of $\underline{E}$ normal to the sunline, as measured by OGO-6, are weaker in the region $\Lambda = 70° - 80°$ in the midnight sector than in the polar cap zone between $\Lambda = 80°$ on the nightside and $\Lambda = 80°$ on the dayside. This is most clearly shown in the analysis by Bohse and Aggson (1973). The third disagreement is with drift paths followed by Ba^+ clouds released in the early morning polar cap. The observed deviations from sun-aligned drift are summarized in Table 2. Although this is a very limited data set, relative to other data quoted here, the observed angles are in agreement with the form of deviation required to remove the objectionable aspects of sun-alignment.

The fact that all three of the above flaws in the sun-aligned models can be compatibly removed by means of the simple modifications shown in Figures 6(c) and 7(c) provides confidence that the modified models are more representative of typical conditions than the sun-aligned models. It is logical to ask if similar modifications are needed on the dayside but the data currently available do not justify significantly changing the modeling practice of drawing sun-aligned streamlines which has been commonly followed since Axford and Hines (1961).

Another logical question appears in looking at the displacement of the evening-morning dividing line in the midnight sector that occurs between Models A and B. Figures 6(a) and 7(a) suggest that the Harang discontinuity, and thus the auroral break-up region, might occur more toward the post-midnight hours in the case of B, and other +Y IMF signatures, than in the

case of A, and other -Y IMF signatures. This possibility was investigated at the time of a previous analysis (Heppner, 1972c) through an extensive examination of the June 1969 auroral belt magnetograms relative to both the polar cap signatures and the azimuthal sector of the IMF. Although shifts were anticipated, systematic differences within the range of short period time variations were not found. Thus, the results were negative and/or inconclusive and were not reported. The consequence for the present modeling is that greater deviations from sun-alignment in the polar cap are required for Model B than for Model A to obtain continuity with the Harang discontinuity region, but no attempt is made to make the Harang discontinuity completely identical in the two models.

Figures 6(d) and 7(d) illustrate the addition of co-rotational potentials to the modified models in Figures 6(c) and 7(c), respectively. The dayside is unmodified from Figures 6(b) and 7(b) but the nightside modifications have a pronounced effect in the midnight sector.

DEVIATIONS FROM MODEL PATTERNS

As explained and estimated in previous sections, Models A and B apply to less than 50 percent of the northern hemisphere data even though they represent the two most common cross-section signatures. This and other expressed qualifications may appear to contradict an earlier statement (Heppner, 1972b) "----that the general pattern of high latitude electric fields in magnetic time-invariant latitude coordinates is not highly variable---." However, the previous statement was made in the context of the existence of a basic two cell convection under both quiet and disturbed conditions and independent of the phase and intensity of individual substorm enhancements. More objectively, the data rule out one cell patterns but do not rule out the

possibility that three or more cells occasionally exist. This is exemplified by cases of signature RC (Heppner, 1972c) in which 3 regions of solar directed convection and 2 regions of anti-solar convection are encountered in crossings between 18^h and 6^h. The more likely alternative to a multi-cell model construction is to assume that such cross-section peculiarities can best be explained in terms of distortions of the basic two cell configuration. This is qualitatively illustrated for the RC signature in Figure 10. An alternative construction for the RC signature, which is regarded here as being equally likely, is given in Langel's (1975) Figure 10. Pattern distortions such as these illustrate why local observations from rockets, balloons, Ba^+ clouds, etc. cannot be used to infer that the overall polar cap convection has switched from being anti-solar to being solar directed.

Other deviations previously noted include: the existence of 8 identifiable signatures in addition to the 4 (A, B, C, RC) illustrated here and the fact that one needs to use combinations of these 12 to classify some cross-sections, a variety of small scale local and regional irregularities which cannot be modeled, and particularly, the prevailing existence of highly irregular fields between 70 and 80° on the dayside in the winter (southern) hemisphere. As the extent of the winter dayside irregularities has not been adequately illustrated in previous publications, Figure 11 is shown here. In this particular case the turbulent appearance is so wide spread that there is no indication of a convection pattern. It is also apparent that local observations would appear unrelated to model patterns.

In contrasting southern (winter) and northern (summer) hemisphere data for passes in the same MLT zone the greater prevalence of irregularities in the winter hemisphere has previously been described. For completeness it should also be noted that whereas sharp, shear-like, field reversals at the polar cap boundary are very rare in the northern (summer) data, there are a number of cases in the southern (winter) hemisphere where this type of boundary occurs on the morning side when the IMF has a +Y component and on the evening side when Y is negative. In these selected cases the field distribution equatorward from the sharp boundary fits the "theory" profile in Figure 1 better than the "observed" profile.

A small magnitude deviation from model profiles, which has not previously been described and does not fit the usual meaning of irregularity, is clearly apparent at the equatorward edge of the morning sunward convection belt on about 10 percent of the OGO-6 passes. The actual frequency of occurrence could be greater than 10 percent because additional questionable cases are influenced by the 5 mv/m uncertainty in the $\underline{v}_s \times \underline{B}$ subtraction for the satellite velocity, $\underline{v}_s$. This deviation is in the form of a zone of poleward $\underline{E}$, anti-solar convection (i.e., instead of going to zero at its low latitude limit the normal equatorward $\underline{E}$ in the morning belt reverses sign and then returns to zero at a lower latitude). The width of this zone is often several degrees in latitude and although magnitudes of about 10 mv/m are most common they sometimes approach 20 mv/m. In the northern hemisphere, where identification is distinct from irregularities, occurrence rates are higher before 5 hours MLT than after and there is a strong tendency for occurrences to be grouped in terms of successive passes. Also in the northern hemisphere, nearly all clear examples occur when the IMF has a -Y component. A comparable deviation

is not observed at the equatorward boundary of the evening sunward convection in either hemisphere or with either sign of the IMF. The geometry for drawing convective continuity to illustrate this deviation is not obvious but it is apparent that it will counteract co-rotation at the equatorward edge of the morning convection when it is present.

The OGO-6 data also show a number of cases where the dawn-dusk component of $\underline{E}$ reverses over a limited latitude range well within the morning and evening belts of sunward convection. Occurrences in the morning belt are more prevalent than in the evening. Most commonly these reversals are not sharp, shear like, features and from examination of simultaneous particle data (courtesy of D. Evans) they do not appear to be closely related to cases where there is an anti-correlation between an intense particle flux and the magnitude of $\underline{E}$. The dimensions, up to several degrees in width, similarly do not suggest a close relationship with auroral forms.

SUMMARY DISCUSSION

The objectives here have been: (1) to provide models of the most simple and frequently occurring field distributions encountered by OGO-6, (2) to make these models as quantitatively accurate and defensible as possible, where possible, such as in cross-section form between 18 and 6 hours MLT, (3) to construct patterns with convective continuity which are representative of observed fields in the nightside auroral belt as well as being quantitatively accurate in dawn-dusk cross-section, (4) to not invoke pattern characteristics deviating from the simplest symmetry in regions where observations do not justify treating a given distortion as being typical (e.g., in the dayside auroral belt), and (5) to

emphasize the limitations of the models and describe the most frequently observed deviations from the model constructions.

The procedure followed has been one of strictly representing the available data and thus it is independent of assumptions as to the cause of the electric field. Most previous models have, directly or indirectly, implied cause: for example, by placing line charges along the polar cap boundary and/or magnetopause boundary with the assumption that these boundaries map into each other. Inasmuch as there are gross differences between boundary characteristics and field distributions in the theoretical and observational models, it is logical to ask if the basic assumptions in such theoretical models are viable. Alternatively, one can ask if the causative mechanisms invoked can be modified and applied to fit observations. Hopefully, the models presented here will stimulate a more realistic application of theory.

The present study reinforces results previously published which showed that the polar cap boundary locations are statistically not closely related to Kp but that Kp is statistically related to the low latitude extension of the auroral belt convection in the dawn-dusk meridian and on the night-side. As previously stated (Heppner, 1973) each two degrees of equatorward displacement is statistically accompanied by an integer increase in Kp but individual cases can differ greatly from averages. Relationships between Kp and the integrated electric field (i.e., total potential) are even more poorly defined. This dependence was previously (Heppner, 1973) roughly estimated to be such that an integer increase in Kp would accompany a 13 kev increase in the total potential with Kp = 0 accompanying a 20 kev total potential. As discussed, the AE index would probably be a more suitable

parameter for correlations but this has not been adequately tested. The present study suggests that 13 kev per integer change in Kp underestimates the total potential and that 20 kev per integer change in Kp is likely to be closer to reality. It does not appear necessary to change the minimum (or base level) total potential of 20 kev at Kp = 0, but the Kp = 0 condition may often accompany total potentials > 20 kev.

Relative to the above, negative results have been obtained in attempts to correlate changes in the low latitude boundary location near noon with magnetic disturbance conditions. The data indicate that the boundary at 12 hours MLT is close to 70° INL at all disturbance levels encountered. This introduces a complication in extrapolating the low latitude boundary in the A and B models to conditions other than Kp = 3 on the basis of the statistical 2 degree change per integer Kp. In essence one needs to introduce a dayside local time dependence which ranges from 2 degrees change per integer Kp at 6 hours and 18 hours to zero change at 12 hours MLT.

The geometrical configuration of convective flow in the region of the Harang discontinuity is such that continuity of flow between the nightside auroral belt and dawn-dusk cross-sections can typically be obtained only by introducing flow configurations in the nightside polar cap which deviate from being directly anti-solar. Roughly characterised, the required deviation is such that nightside flow streamlines tend to parallel the 10 hour to 22 hour MLT meridian rather than the 12 hour to 24 hour MLT meridian. This generalization is also supported by observations of Ba^+ clouds released in the early morning polar cap.

The most deficient aspect of the present modeling could be that it applies directly only to the summer northern hemisphere. As this aspect

has not been discussed as extensively as the various observed deviations from the model patterns, additional comment is appropriate. In terms of existing data and analyses of polar cap asymmetries related to the sign of the Y-component of the IMF (Heppner: 1972c, 1973) it is logical to assume that Model B applies in the southern hemisphere when Model A applies in the northern hemisphere, and vice versa. This co-existence of contrasting asymmetries (e.g., signatures A, D, or E in the northern hemisphere with B, C, SC, or RC in the southern hemisphere, and vice-versa, Heppner, 1972c) will introduce uncertainties when one attempts to construct magnetospheric models by extrapolation. For example, even though the total potential is 76 kev in both, A and B, cases there are 2 kev differences in the potential changes across the evening and morning auroral belts, respectively, in the two hemispheres. Similarly, there are differences of a fraction of a degree in the low latitude convection boundary where conjugacy is expected. These small differences could be either real or merely a consequence of the data selection and statistics; this is indeterminant. The principal uncertainty appears when one attempts to reconcile having the two patterns (A as shown in Figures 6a or 6c and B as shown in Figures 7a or 7c) co-exist in opposite hemispheres. This problem is left open in the present analysis because finding a solution involves a series of assumptions keyed to magnetic field distortions in outer magnetospheric regions. It is outside the scope of this paper to go beyond stating that complex magnetospheric field distortions are required.

REFERENCES

Axford, W. I. and C. O. Hines, A unifying theory of high-latitude geophysical phenomena and geomagnetic storms, Can. J. Phys., 39, 1433, 1961.

Bohse, J. R. and T. L. Aggson, Average ionospheric electric field distribution, EOS, 54, 417, 1973.

Cauffman, D. P. and D. A. Gurnett, Satellite measurements of high latitude convection electric fields, Space Sci. Reviews, 13, 369, 1972.

Gurnett, D. A., Electric field and plasma observations in the magnetosphere, in Critical Problems of Magnetospheric Physics, ed. by E. R. Dyer, p. 123, Nat. Acad. of Sci., Washington, D. C., 1972.

Heppner, J. P., J. D. Stolarik, and E. M. Wescott, Electric field measurements and the identification of currents causing magnetic disturbances in the polar cap, J. Geophys. Res., 76, 6028, 1971.

Heppner, J. P., The Harang discontinuity in auroral belt ionospheric currents, Geofysiska Publikasjoner, 29, 105, 1972a.

Heppner, J. P., Electric field variations during substorms: OGO-6 measurements, Planet. Space Sci., 20, 1475, 1972b.

Heppner, J. P., Polar-cap electric field distributions related to the interplanetary magnetic field direction, J. Geophys. Res., 25, 4877, 1972c.

Heppner, J. P., Electric fields in the magnetosphere, in Critical Problems of Magnetospheric Physics, ed. by E. R. Dyer, p. 107, Nat. Acad. of Sciences, Washington, D. C., 1972d.

Heppner, J. P., High latitude electric fields and the modulations related to interplanetary magnetic field parameters, Radio Sci., 8, 933, 1973.

Kawasaki, K., A model of the electric field over the polar cap, Rep. Ionos. Space Res. Japan, 29, 157, 1975.

Langel, R. A., A comparison of electric and magnetic field data from the OGO-6 spacecraft, J. Geophys. Res., 80, 4661, 1975.

Maeda, H., Neutral winds and ion drifts in the polar ionosphere caused by convection electric fields, J. Atmos. Terr. Phys., 38, 197, 1976.

Maynard, N. C., Electric field measurements across the Harang discontinuity, J. Geophys. Res., 79, 4620, 1974.

Olson, W. P., Summary of the La Jolla conference on quantitative magnetospheric models, EOS, 56, 607, 1975.

Volland, H., Models of global electric fields within the magnetosphere, Ann. Geophys., 159, 1975.

Wolf, R. A., Calculation of magnetospheric electric fields, in Magnetospheric Physics, ed. by B. M. McCormac, p. 167, D. Reidel Publ., Co, Dordrecht-Holland, 1974.

FIGURE CAPTIONS

Figure 1: Illustrative comparison of an empirically modeled (observed) and a theoretical cross-section of the electric field in the dawn-dusk meridian. +E is directed from dawn toward dusk normal to the sun-line.

Figure 2: Dawn-dusk model cross-section in the northern hemisphere for cases when the polar cap field has signature A and the IMF is in the -Y hemisphere.

Figure 3: Dawn-dusk model cross-section in the northern hemisphere for cases when the polar cap has signature B and the IMF is in the +Y hemisphere.

Figure 4: Dawn-dusk model cross-section from successive northern hemisphere traverses showing signature C during a quiet, Kp = 0. period when the IMF was in the +Y hemisphere.

Figure 5: Dawn-dusk model cross-section from successive northern hemisphere traverses during a disturbed, AE = 1000, period when the IMF was in the -Y hemisphere.

Figure 6: Convection patterns based on Model A (4 kev contour intervals):

(a) Sun-aligned pattern. The dashed line shows the location of the polar cap boundary.

(b) Sun-aligned pattern with co-rotation added.

(c) "A" pattern modified to fit nightside observations. The Harang discontinuity is indicated with a dashed line.

(d) "A" pattern modified to fit nightside observations with co-rotation added.

Figure 7: Convection patterns based on Model B (4 kev contour intervals)

(a) Sun-aligned pattern. The dashed line shows the location of the polar cap boundary.

(b) Sun-aligned pattern with co-rotation added.

(c) "B" pattern modified to fit nightside observations. The Harang discontinuity is indicated with a dashed line.

(d) "B" pattern modified to fit nightside observations with co-rotation added.

Figure 8: A sun-aligned representation of Model C(0) with 2 kev contour intervals.

Figure 9: A sun-aligned representation of Model AD with 8 kev contour intervals.

Figure 10: A mode of distorting a 2 cell pattern to produce signature RC.

Figure 11: An example of highly irregular electric fields in the dayside winter hemisphere.

Table 1: Parameters for Models A and B

	Boundaries INL (degrees)				Location of Peak Magnitude INL (degrees)			Peak Magnitude volts/km			Potential Difference (volts)		
	$\Lambda(18)$	$\Lambda(P18)$	$\Lambda(P6)$	$\Lambda(6)$	$\lambda(18)$	$\lambda(P)$	$\lambda(6)$	E(18)	E(P)	E(6)	$\int_{18} E \cdot dl$	$\int_{P} E \cdot dl$	$\int_{6} E \cdot dl$
Mean	61.6	74.2	74.9	64.5	68.9		70.8	53.5	30.9*	58.0	40780.		36490.
Model A								53.	21.6	57.	40000.	76000.	36000.
σ	2.6	2.1	2.0	3.3	2.7		2.2	21.	6.*	22.			
Mean	61.9	77.7	73.5	63.8	70.4	78.3	71.7	44.3	48.1	58.7	42350.	83810.	34450.
Model B								44.	43.6	58.	42000.	76000.	34000.
σ	2.9	4.4	2.1	2.8	2.9	2.2	2.3	16.	15.	18.			

* limited meaning

Table 2: Polar Cap Ion Cloud Drift Directions

Date	Cloud	Release Point: Invariant Latitude (degrees)	Release Point: Magnetic Local Time	Average angle* between the ion cloud path and the anti-solar direction (degrees)
			Evening	
3-20-71	1	80.5	19:04	- 19.0
(K_p=4$^-$)	2	80.7	18:53	- 20.6
	3	80.9	18:45	- 20.4
	4	81.1	18:35	- 18.9
3-8-69**	1	75.9	16:42	7.7
(K_p= 3)	2	76.5	16:44	4.9
	3	77.1	16:45	8.4
	4	77.8	16:47	15.1
			Morning	
3-15-71	1	80.6	3:15	30.1
(K_p=4$^+$)	2	80.9	3:05	- 26.9
	3	81.1	2:57	- 15.5
	4	81.4	2:47	- 14.7
3-19-71	1	80.4	2:44	- 24.7
(K_p= 1)	2	80.6	2:37	- 32.2
	3	80.8	2:30	- 28.4
	4	80.9	2:21	- 19.4
3-7-69**	1	75.7	2:38	- 21.0
(K_p=3$^+$)	2	76.2	2:38	- 39.9
	3	76.7	2.38	- 42.4
	4	77.2	2:38	- 35.2

* negative values are clockwise from the anti-solar direction when viewed from above the north pole.
** tracks are illustrated in Heppner et al. (1971)

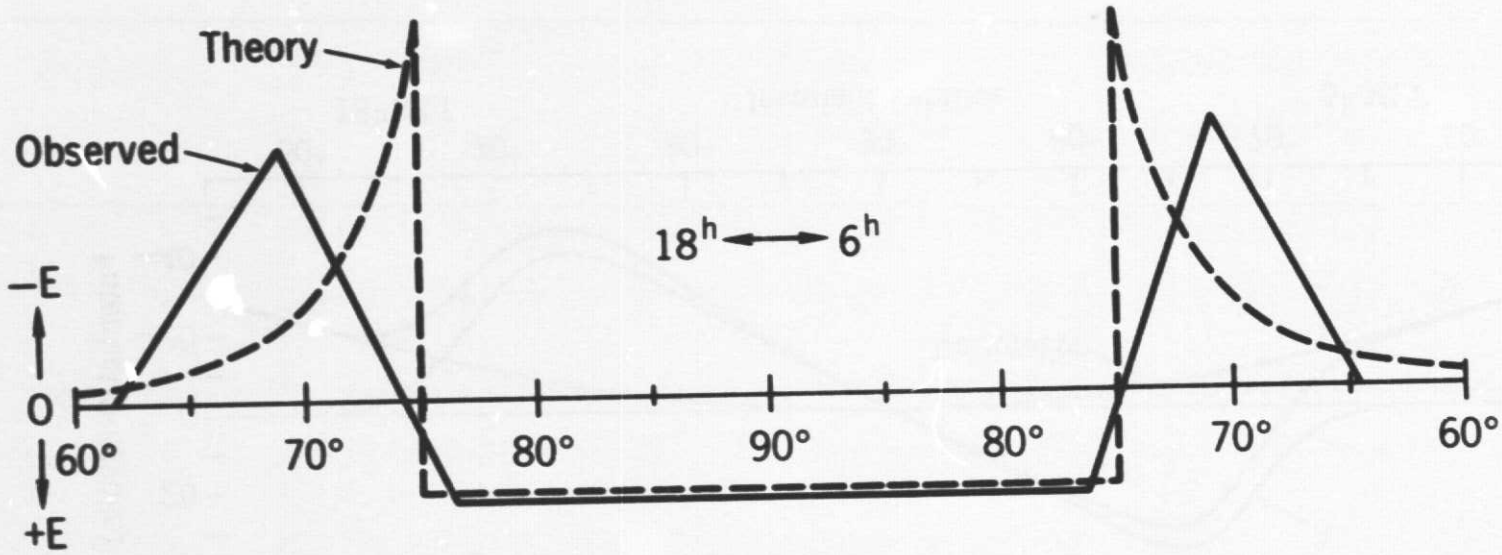

Figure 1

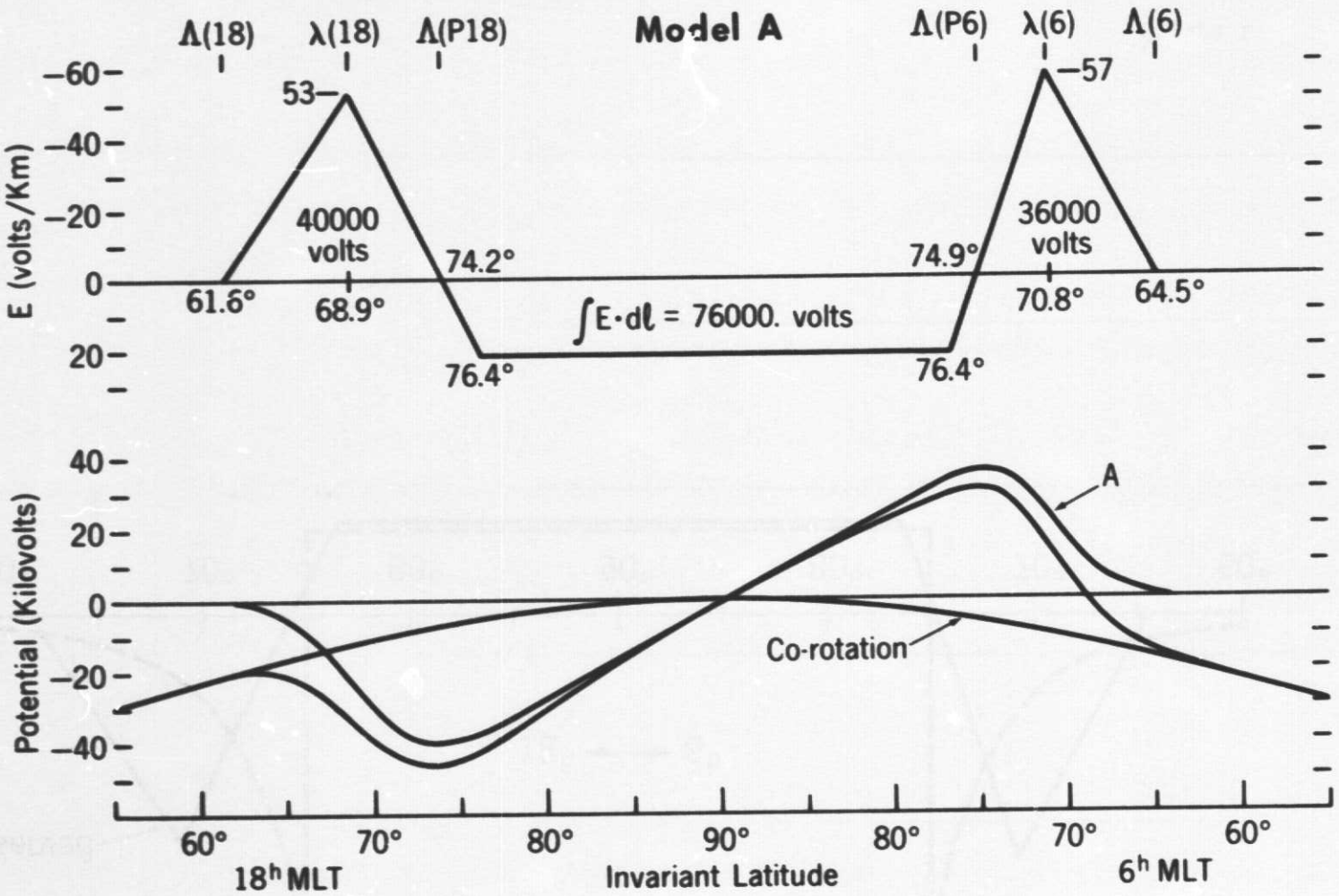
Model A
Λ(18)
λ(18)
Λ(P18)
Λ(P6)
λ(6)
Λ(6)
E (volts/Km)
−60
−40
−20
0
20
53
−57
40000 volts
36000 volts
61.6°
68.9°
74.2°
74.9°
70.8°
64.5°
76.4°
76.4°
∫E·dl = 76000. volts
Potential (Kilovolts)
40
20
0
−20
−40
A
Co-rotation
60°
70°
80°
90°
80°
70°
60°
18h MLT
Invariant Latitude
6h MLT

Figure 2

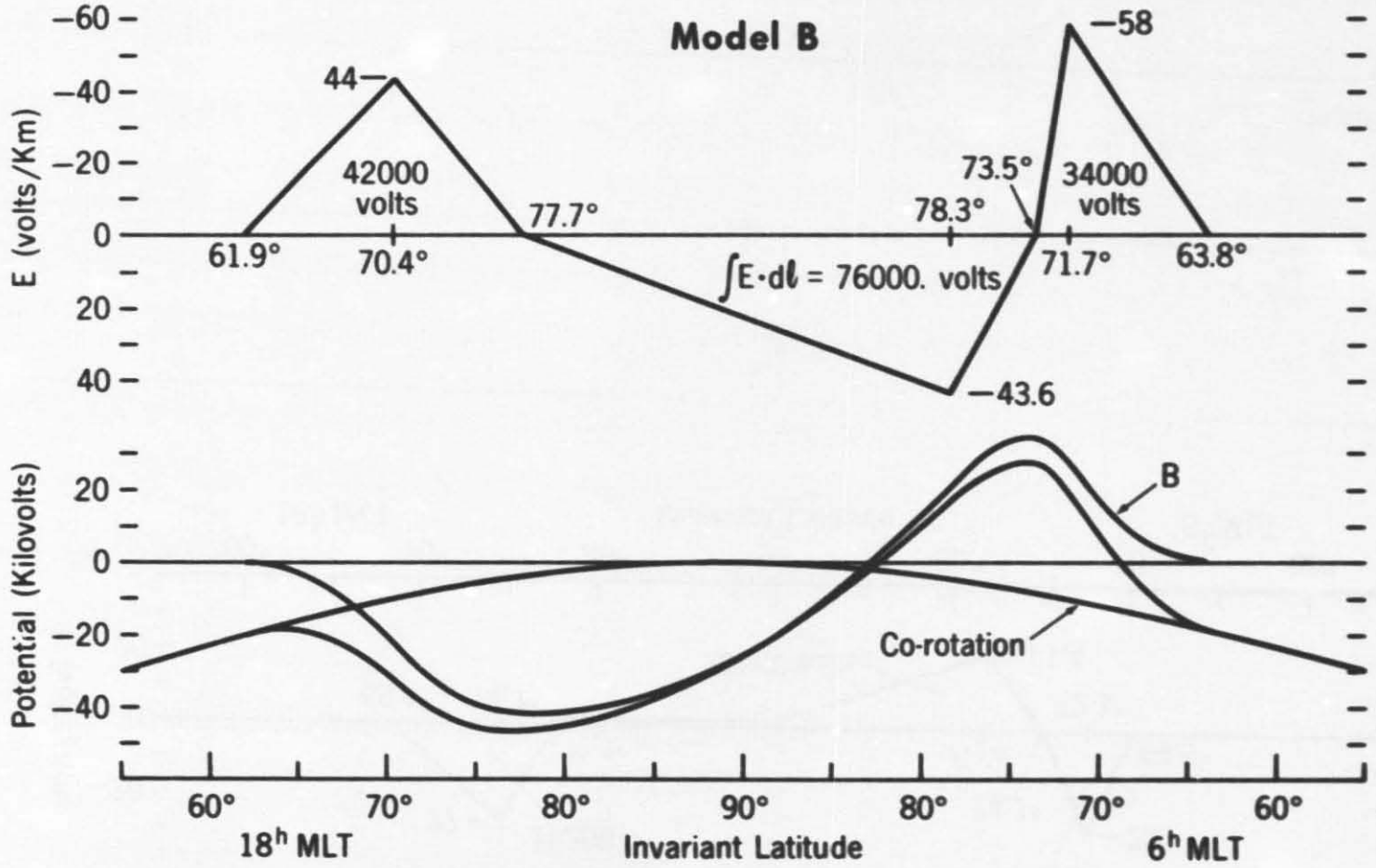
Model B
E (volts/Km)
−60
−40
−20
0
20
40
44
42000
volts
61.9°
70.4°
77.7°
78.3°
73.5°
−58
34000
volts
71.7°
63.8°
∫E·dℓ = 76000. volts
−43.6
Potential (Kilovolts)
20
0
−20
−40
B
Co-rotation
60°
70°
80°
90°
80°
70°
60°
18h MLT
Invariant Latitude
6h MLT

Figure 3

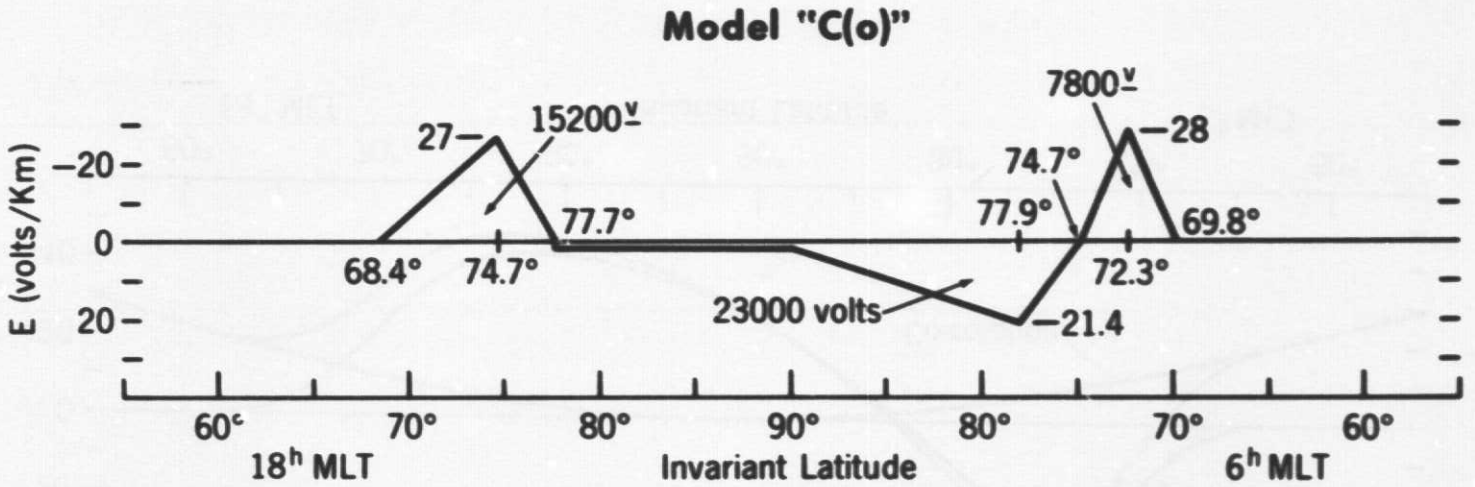
Model "C(o)"
E (volts/Km)
-20
0
20
27
15200 v
77.7°
68.4°
74.7°
7800 v
28
74.7°
77.9°
69.8°
72.3°
23000 volts
21.4
60°
70°
80°
90°
80°
70°
60°
18h MLT
Invariant Latitude
6h MLT

Figure 4

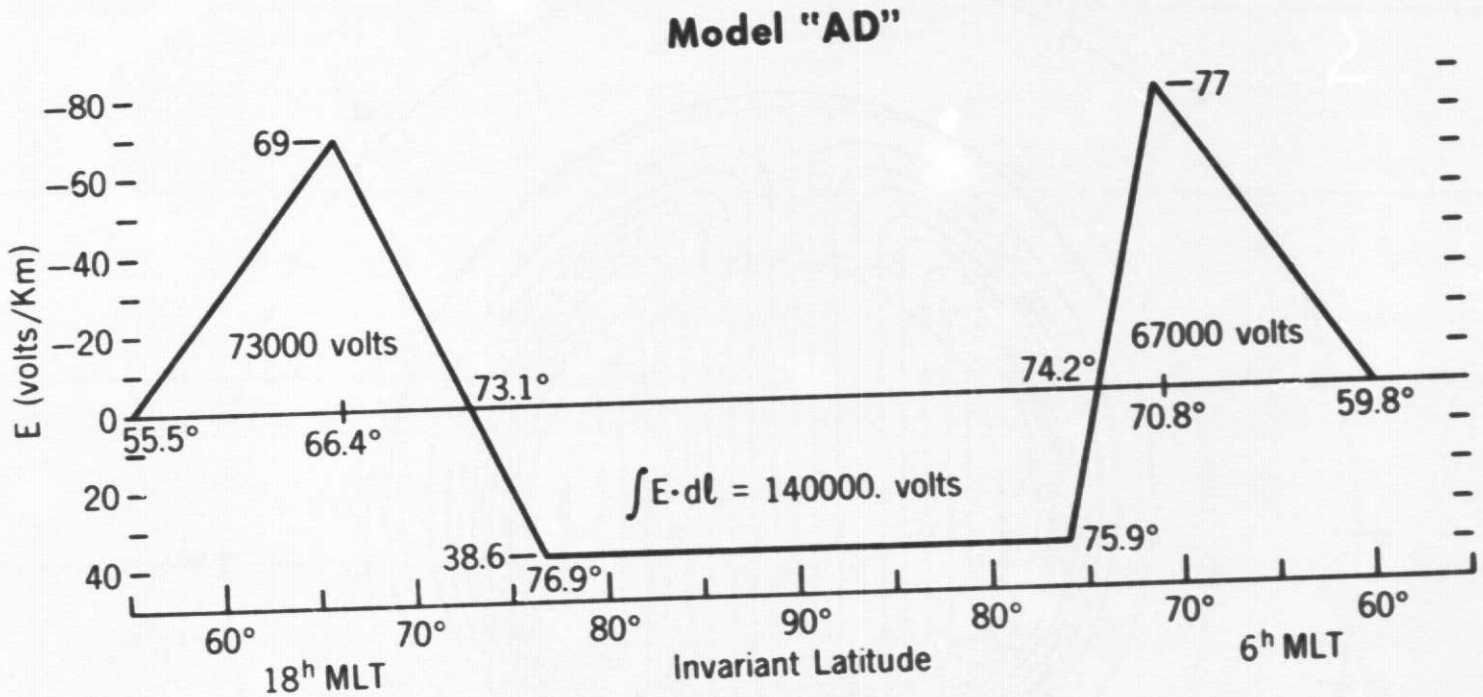
Model "AD"
E (volts/Km)
−80
−50
−40
−20
0
20
40
69
−77
73000 volts
67000 volts
55.5°
66.4°
73.1°
74.2°
70.8°
59.8°
∫E·dl = 140000. volts
38.6
76.9°
75.9°
60°
70°
80°
90°
80°
70°
60°
18h MLT
Invariant Latitude
6h MLT

Figure 5

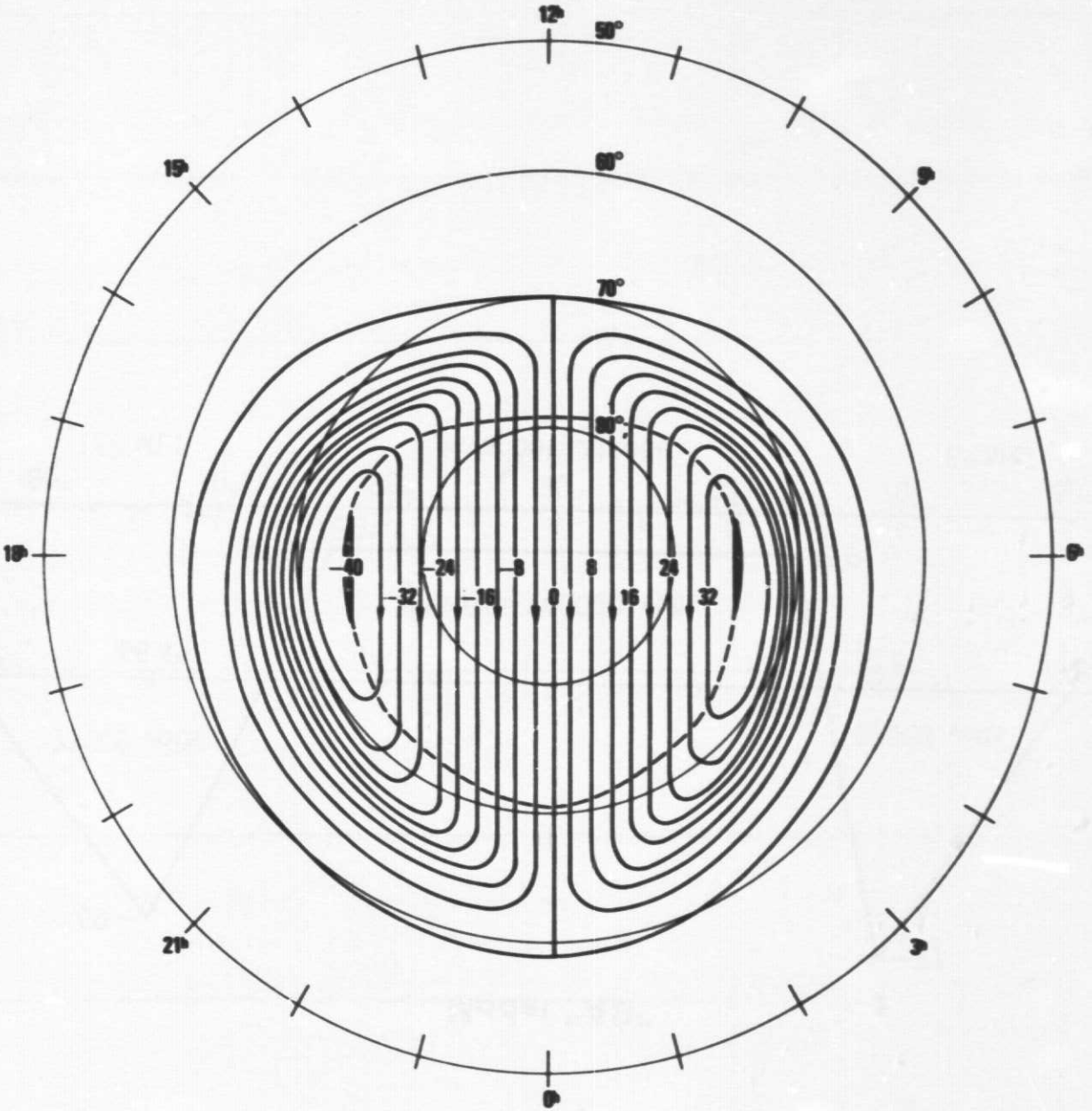

(a) MODEL "A": SUN-ALIGNED

Figure 6 (a)

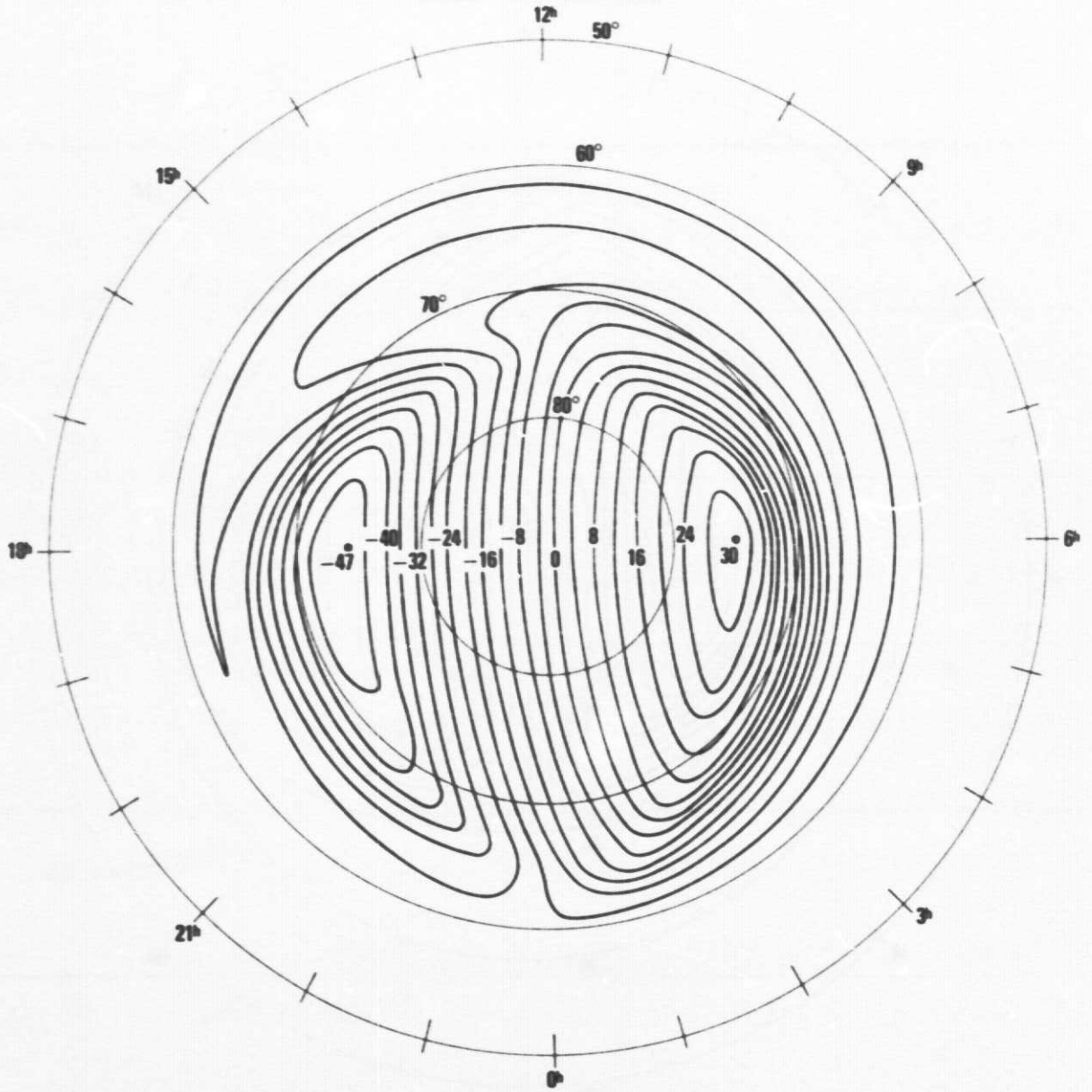

(b) MODEL "A": SUN-ALIGNED WITH CO-ROTATION POTENTIAL

Figure 6 (b)

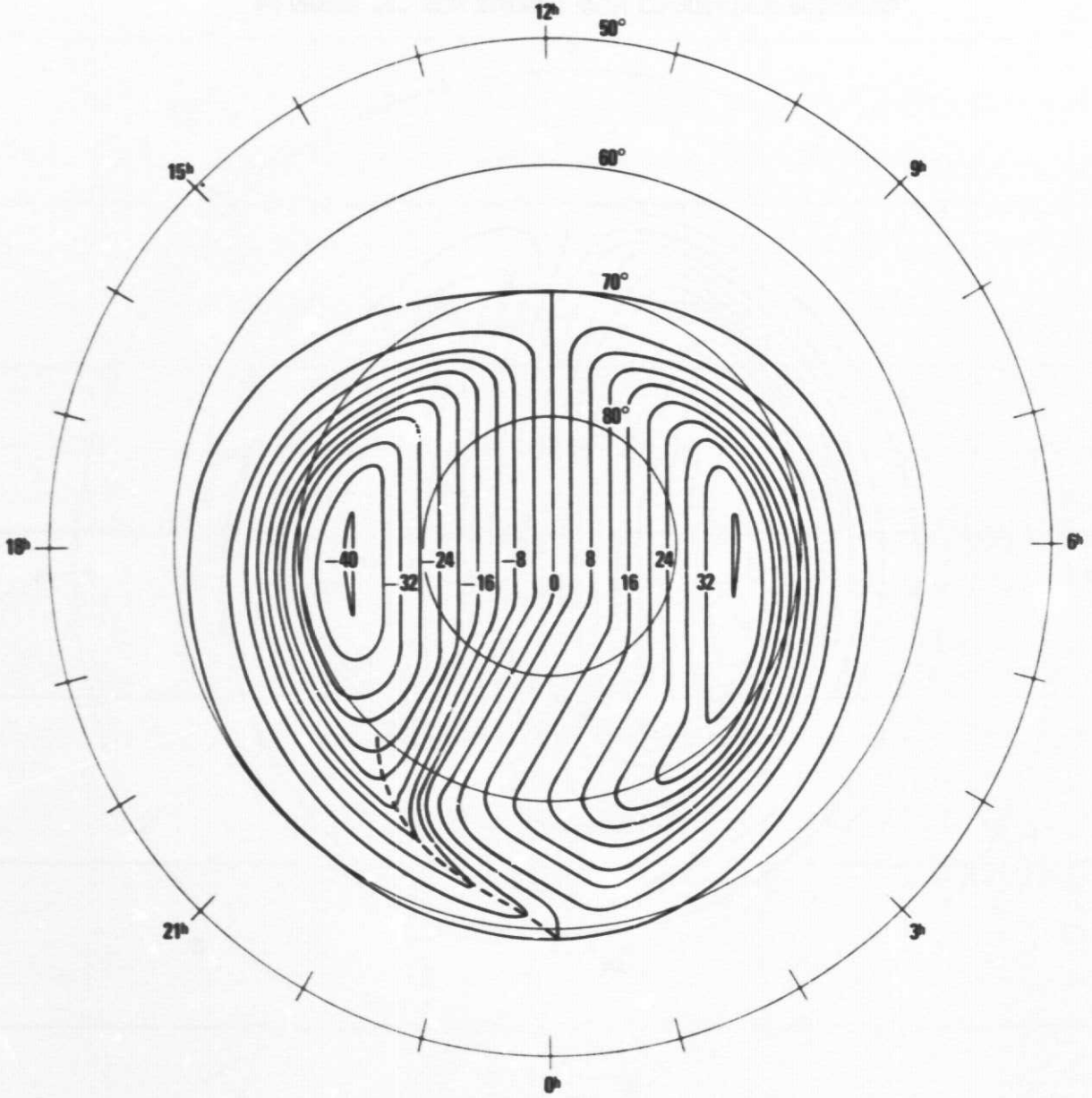

(c) MODEL "A": MODIFIED

Figure 6 (c)

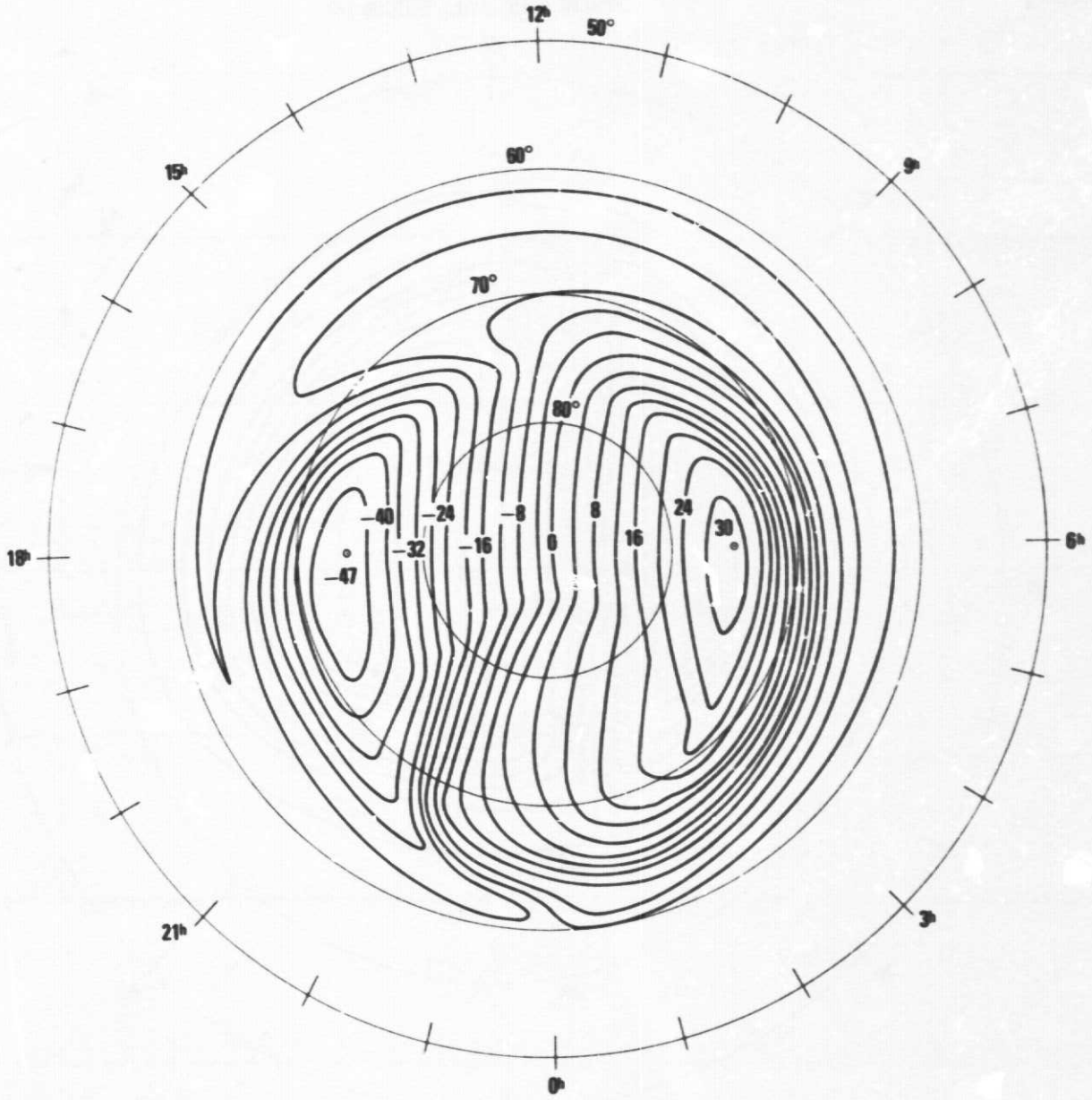

(d) MODEL "A": MODIFIED WITH CO-ROTATION POTENTIAL

Figure 6 (d)

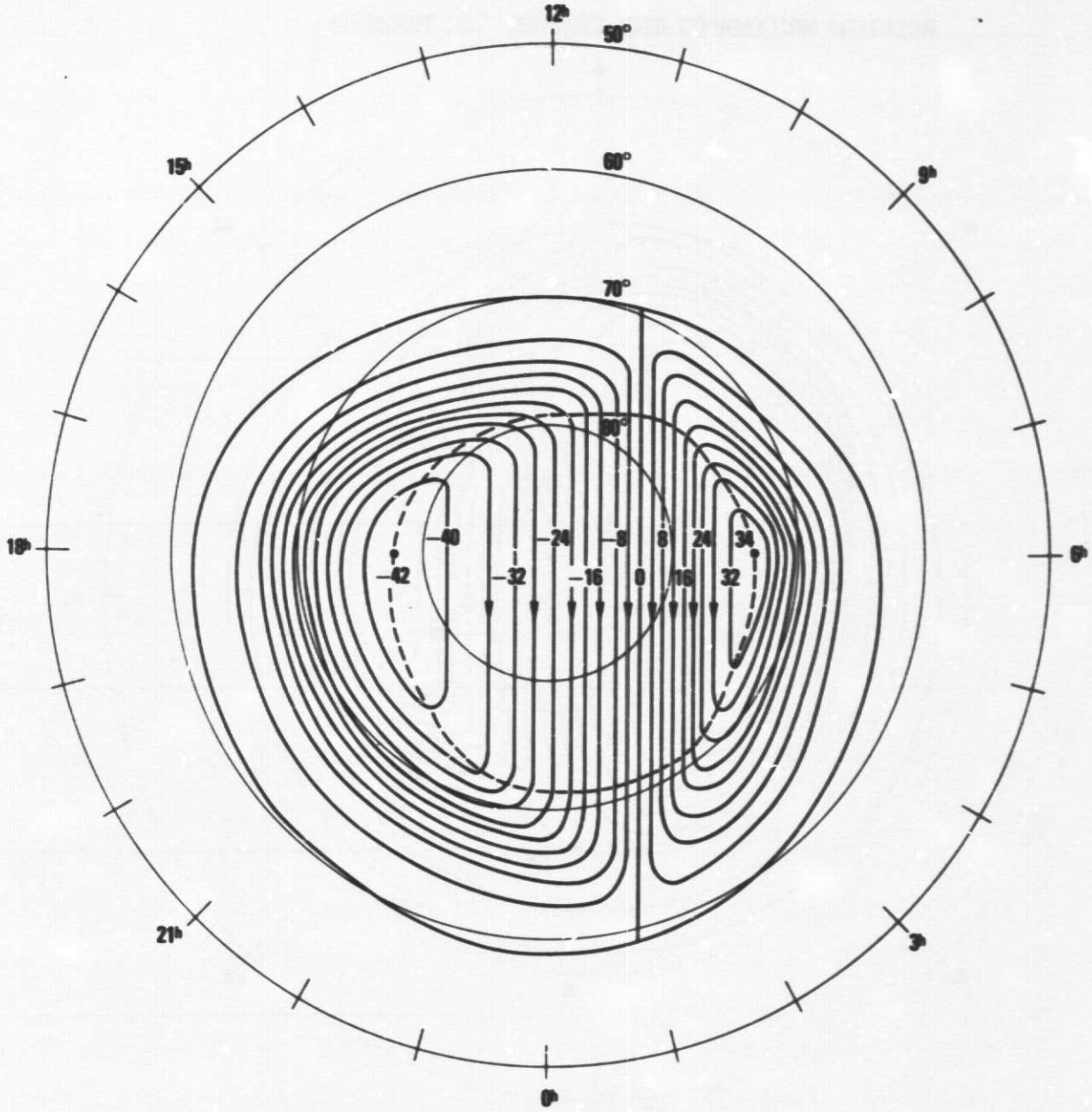

(a) MODEL "B": SUN-ALIGNED

Figure 7 (a)

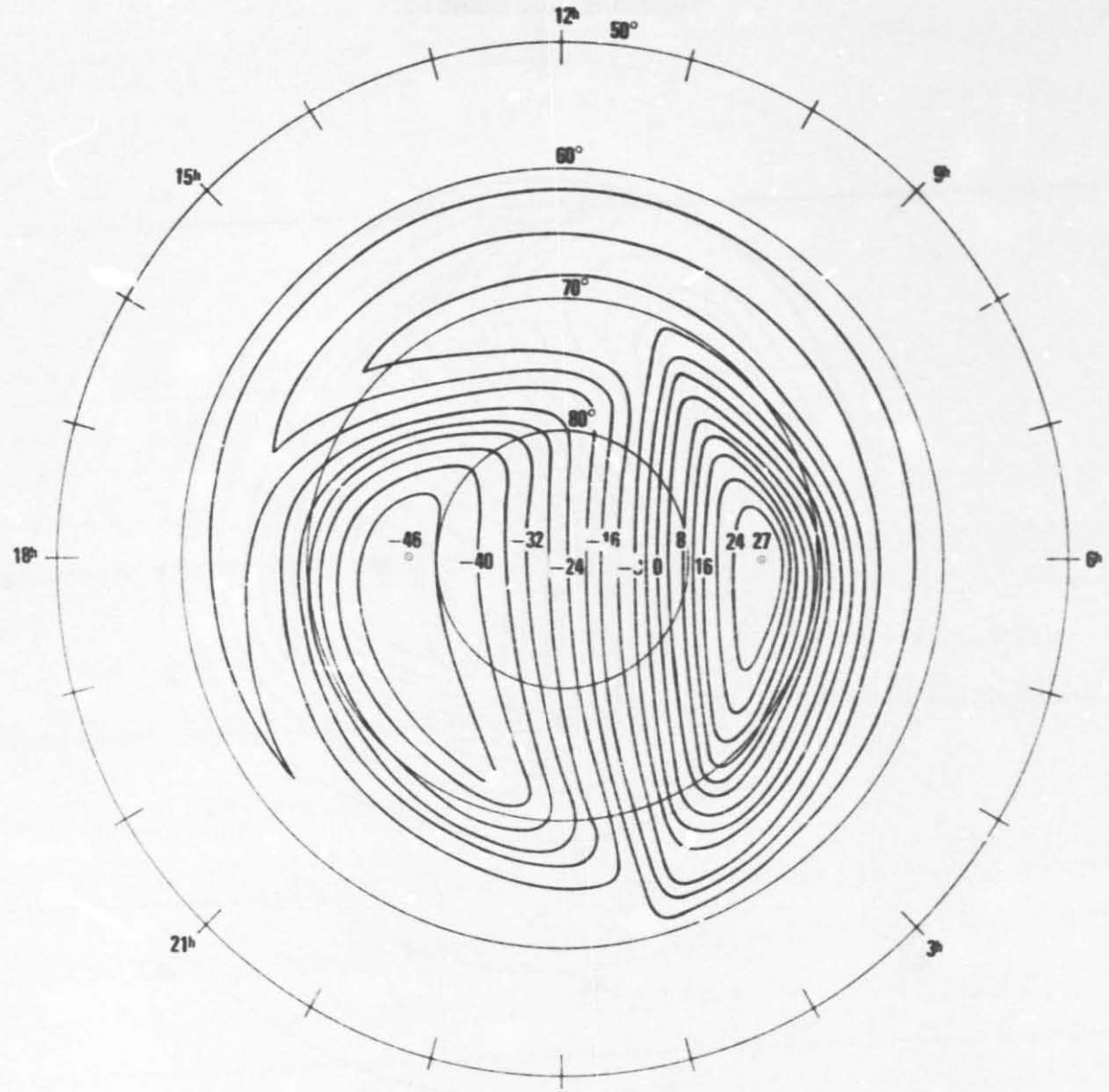

(b) MODEL "B": SUN-ALIGNED WITH CO-ROTATION POTENTIAL

Figure 7 (b)

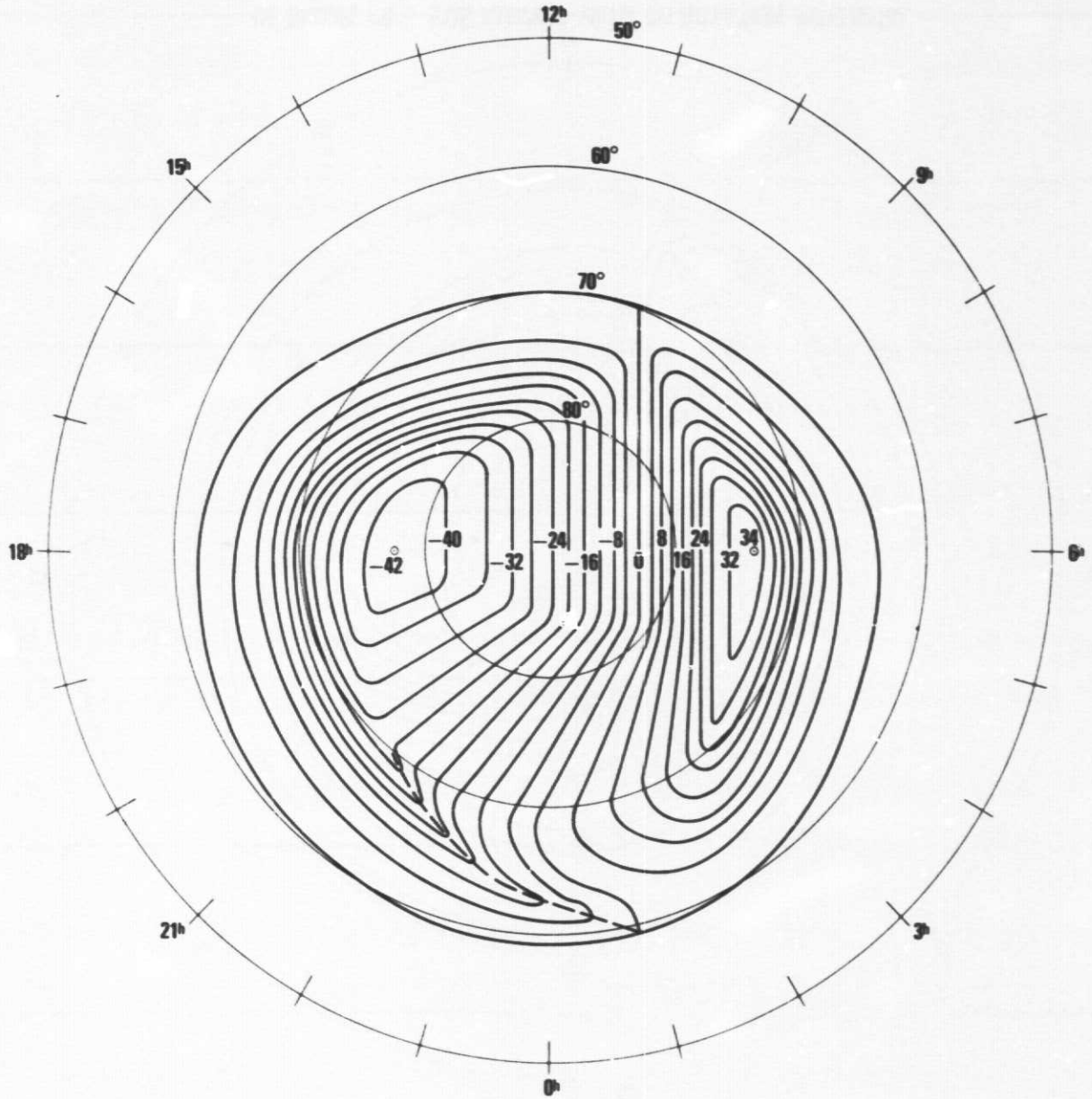

(c) MODEL "B": MODIFIED

Figure 7 (c)

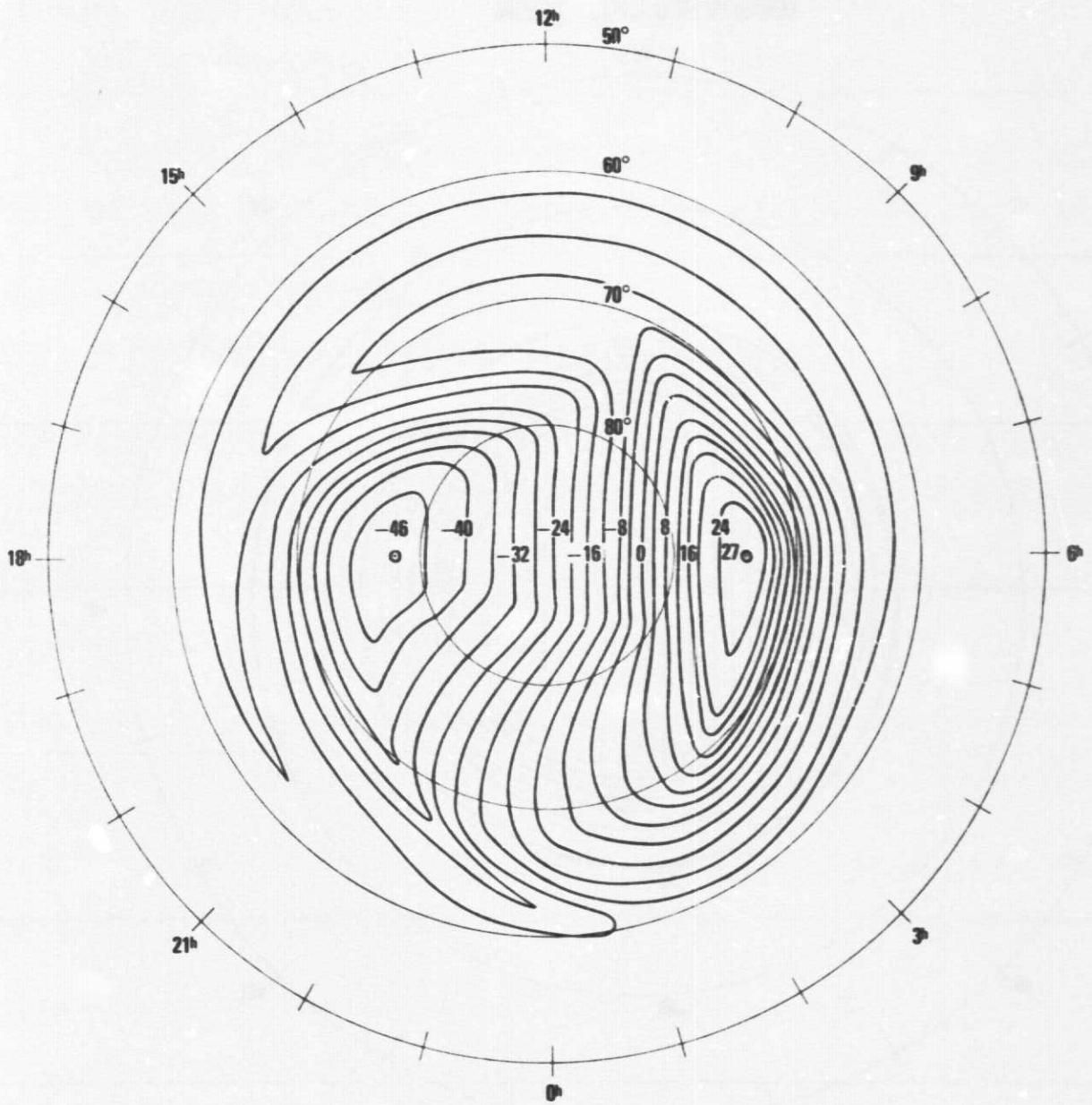

(d) MODEL "B": MODIFIED WITH CO-ROTATION POTENTIAL

Figure 7 (d)

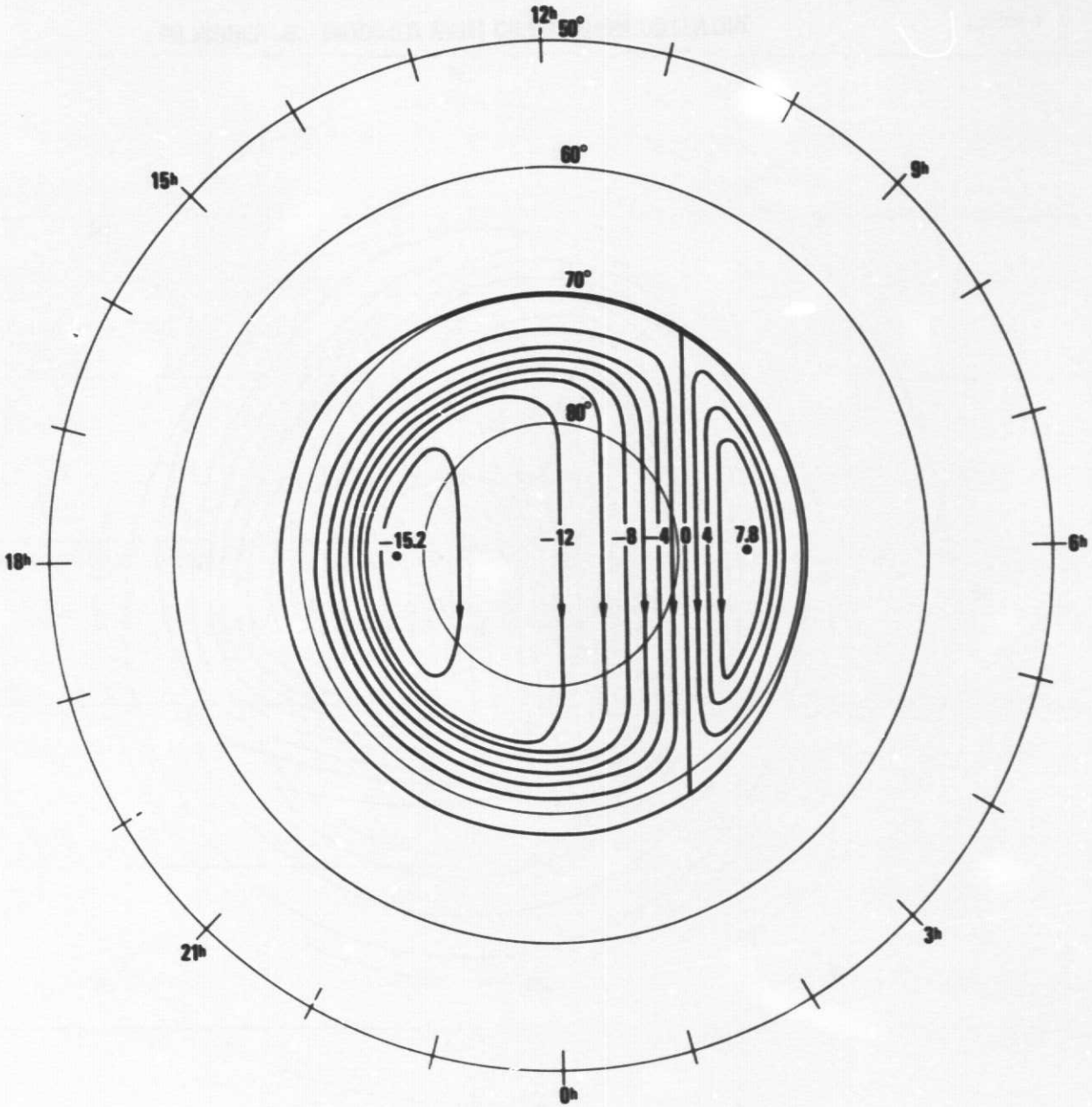

MODEL "C(o)": SUN-ALIGNED

Figure 8

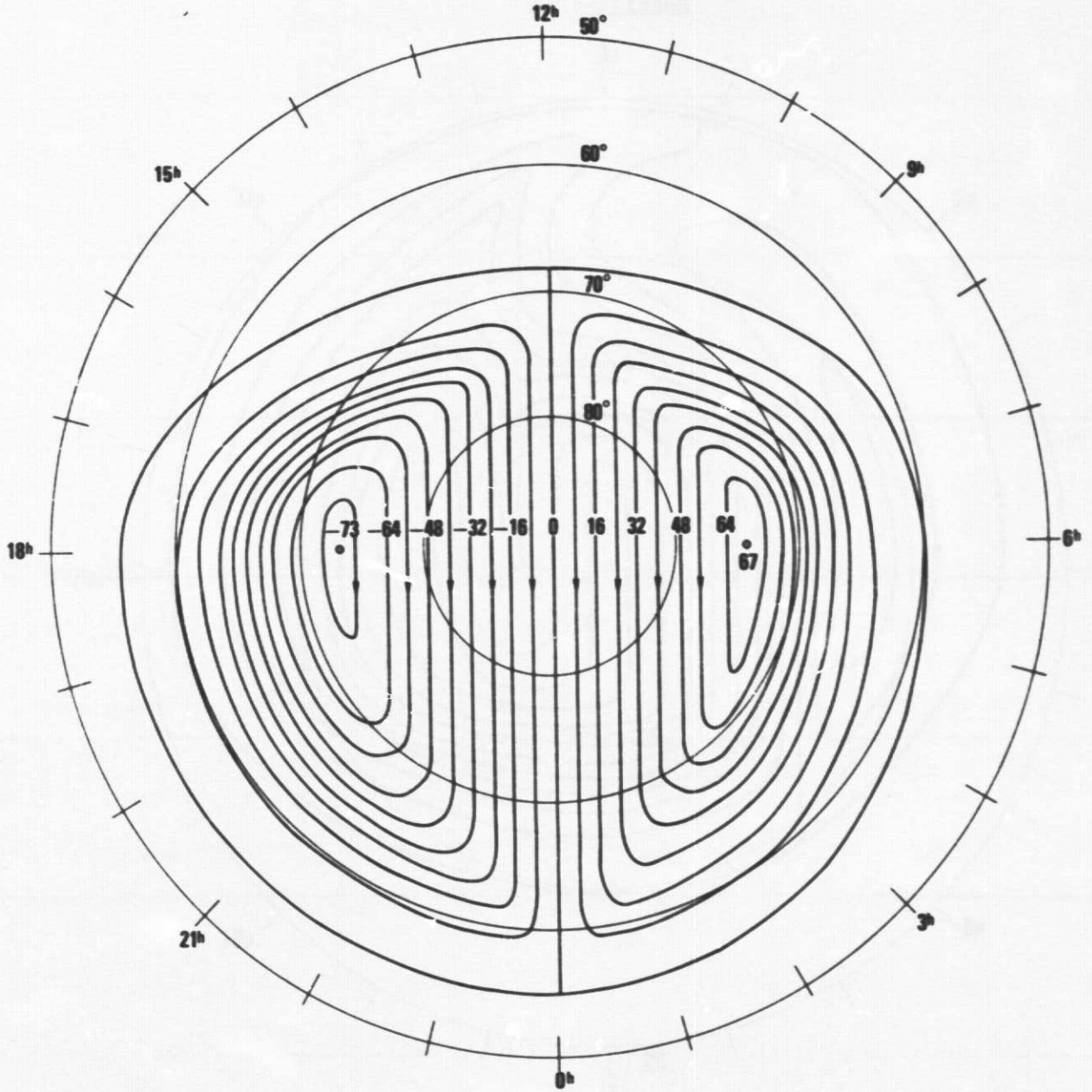

MODEL "AD": SUN-ALIGNED

Figure 9

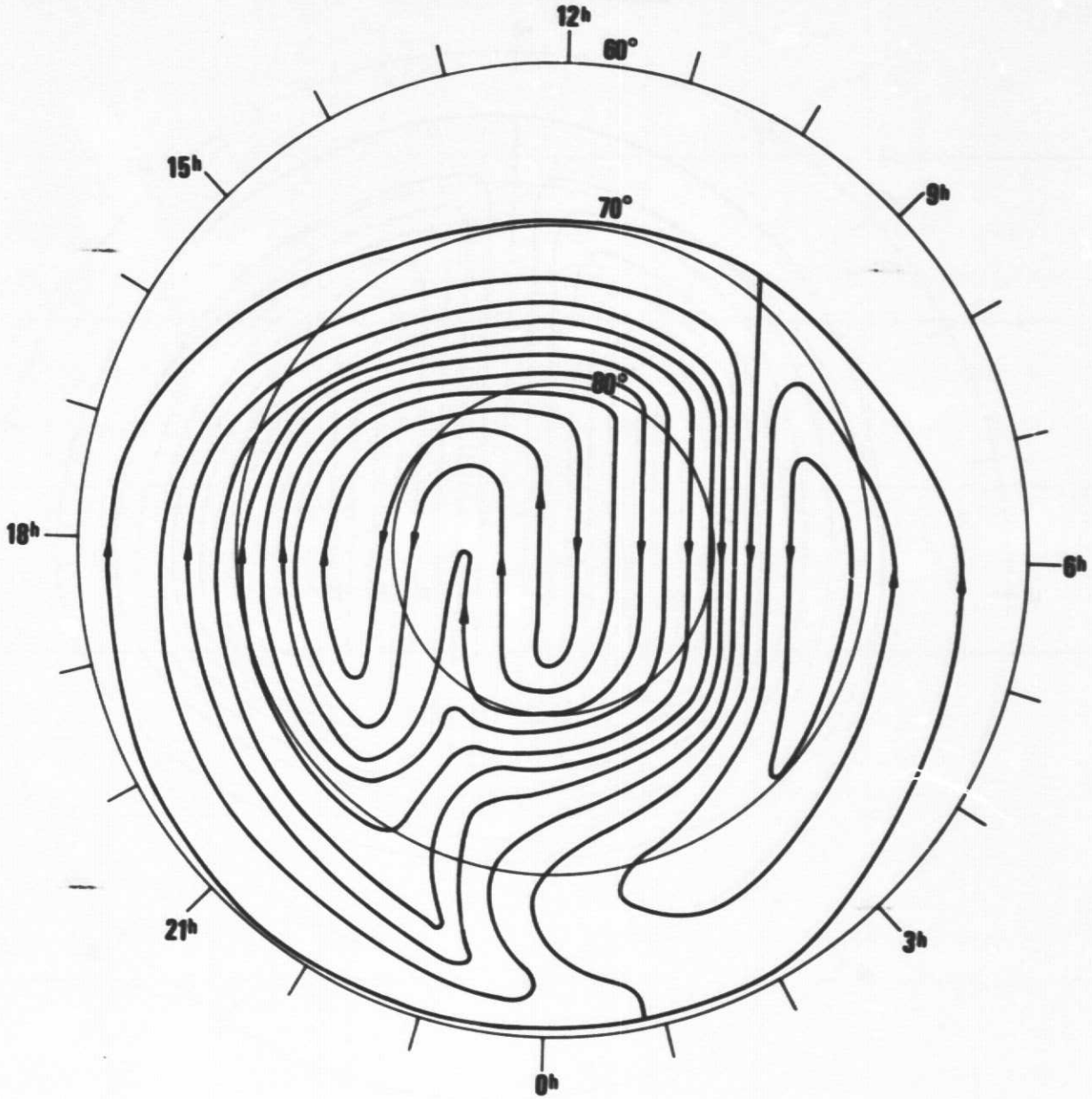

RC PATTERN

Figure 10

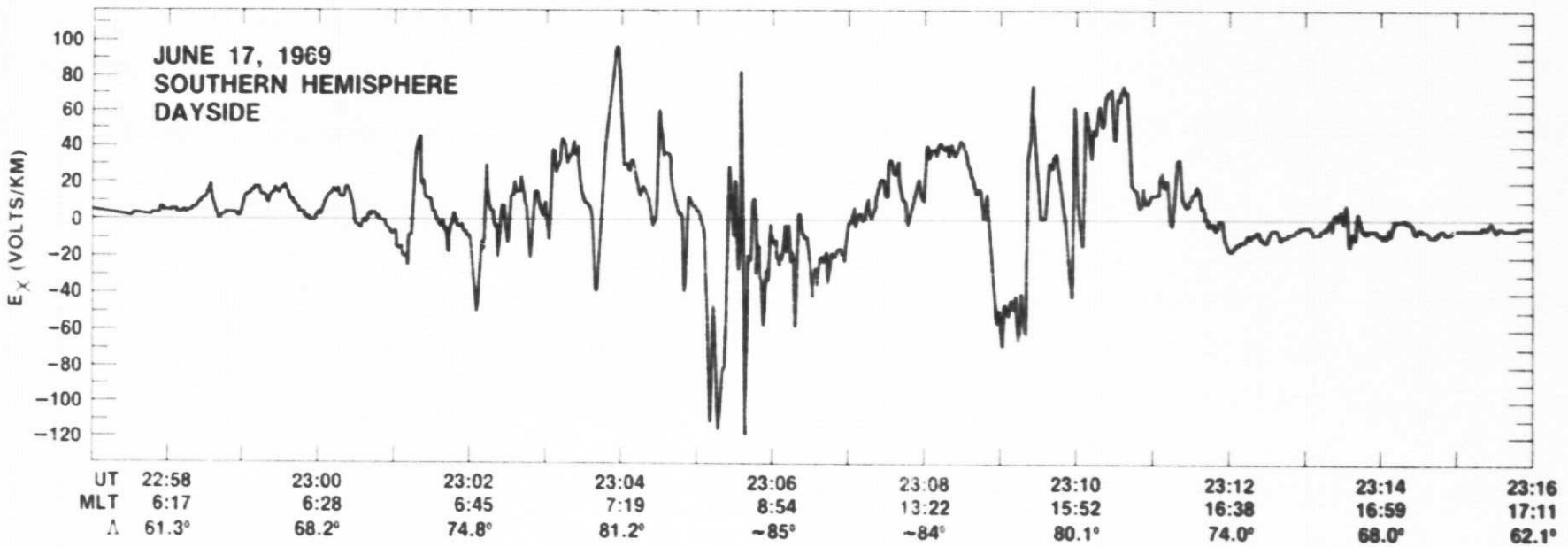
JUNE 17, 1969
SOUTHERN HEMISPHERE
DAYSIDE
E_χ (VOLTS/KM)
100
80
60
40
20
0
-20
-40
-60
-80
-100
-120
UT 22:58 23:00 23:02 23:04 23:06 23:08 23:10 23:12 23:14 23:16
MLT 6:17 6:28 6:45 7:19 8:54 13:22 15:52 16:38 16:59 17:11
Λ 61.3° 68.2° 74.8° 81.2° ~85° ~84° 80.1° 74.0° 68.0° 62.1°

Figure 11